ADVANCED OPTICAL MATERIALS
www.advopticalmat.de

All-Optical Helicity-Dependent Switching in Hybrid Metal–Ferromagnet Thin Films

Feng Cheng, Zhidong Du, Xinjun Wang, Ziqiang Cai, Lin Li, Chuangtang Wang, Abdelkrim Benabbas, Paul Champion, Nianxiang Sun, Liang Pan, and Yongmin Liu**

Over the past decades, optical manipulation of magnetization by ultrafast laser pulses has attracted extensive interest. It not only shows intriguing fundamental science arising from the interactions between spins, electrons, phonons, and photons, but also manifests the potential to process and store data at a speed that is three orders of magnitude faster than the current technologies. In this paper, all-optical helicity-dependent switching (AO-HDS) in hybrid metal–ferromagnet thin films, which consist of Co/Pt multilayers with perpendicular magnetic anisotropy and an Au film capping layer on the top, is experimentally demonstrated. The switching behaviors of the hybrid Co/Pt–Au material, with various laser repetition rates, scanning speeds, and fluencies, are systematically studied. In comparison with bare Co/Pt multilayers, the hybrid metal–ferromagnet thin films show pronounced AO-HDS when the number of laser pulses per μm along the scanning direction gradually increases. In addition, the AO-HDS effect is very robust against laser fluences. A possible mechanism is further proposed based on numerical simulations of the optomagnetic coupling model. These findings promise a new material system that exhibits stable AO-HDS phenomena, and hence can transform future magnetic storage devices, especially with the addition of plasmonic nanostructures made of noble metals.

The demands for high-rate and high-density data storage have been explosively increasing in the current Big Data era. Recent research has shown that ultrafast circularly polarized laser pulses are able to switch the magnetization in certain magnetic thin films with perpendicular magnetic anisotropy. More specifically, right circularly polarized (RCP) and left circularly polarized (LCP) pulses can deterministically switch magnetization without any external magnetic fields that otherwise exist in conventional magnetic storage devices. This is termed all-optical helicity-dependent switching (AO-HDS). Such a novel effect could substantially improve the speed of data storage and information processing technologies, leveraging it from a few gigahertz to the unprecedented terahertz region.

The advancement of AO-HDS has been closely related to materials engineering. The phenomenon of AO-HDS was initially found in ferrimagnetic systems involving rare earth and transition metal (RE-TM) elements,[1–15] in which two distinct sublattices are anti-ferromagnetically exchange coupled. So far, people have found different methods to manipulate AO-HDS in ferrimagnetic materials; for instance, by engineering suitable constituent concentration,[2–5] changing ambient temperature,[6–8] using a substrate with high thermal conductivity,[16] or tuning incident laser parameters.[10,11] Very recently, AO-HDS has been demonstrated in rare-earth-free ferromagnetic materials, such as Co/Pt, Co/Ni multilayers, and granular FePt films,[17–24] which are particularly important to magnetic data storage. Measurements from Hall cross[21,25] and magneto-optical Kerr effect (MOKE)[20,23,24] microscopy reveal that helicity-dependent switching in ferromagnetic materials requires accumulative laser pulses, distinctly different from the switching in ferrimagnetic materials. Interestingly, time-resolved MOKE measurements with a single laser pulse have shown that magnetic dynamics is independent of helicity.[20,26] Despite the significant progress achieved in this field, the underlying mechanism of AO-HDS is still not conclusive. AO-HDS can be explained by the inverse Faraday effect (IFE),[27–30] in which RCP (LCP) laser pulses generate magnetic fields antiparallel (parallel) to the wave vector and trigger helicity-dependent magnetic switching. Another potential

F. Cheng, Dr. X. Wang, Z. Cai, C. Wang, Prof. N. Sun, Prof. Y. Liu
Department of Electrical and Computer Engineering
Northeastern University
Boston, MA 02115, USA
E-mail: y.liu@northeastern.edu

Dr. Z. Du, Prof. L. Pan
School of Mechanical Engineering and Birck Nanotechnology Center
Purdue University
West Lafayette, IN 47907, USA
E-mail: liangpan@purdue.edu

Dr. L. Li, Prof. Y. Liu
Department of Mechanical and Industrial Engineering
Northeastern University
Boston, MA 02115, USA

Dr. A. Benabbas, Prof. P. Champion
Department of Physics
Northeastern University
Boston, MA 02115, USA

The ORCID identification number(s) for the author(s) of this article can be found under https://doi.org/10.1002/adom.202000379.

DOI: 10.1002/adom.202000379

mechanism is the magnetic circular dichroism (MCD).[12,23,31,32] Magnetization (up or down) has slightly different switching probabilities when exposed to circularly polarized light with opposite helicities. This effect accumulates with consecutive pulses and eventually leads to helicity-dependent switching. In addition, the existence of spin–orbit interactions[33–35] and laser-induced superdiffusive spin currents[36,37] in heterogeneous systems has been reported, which may contribute to the AO-HDS process.

In this paper, we experimentally demonstrate AO-HDS in hybrid metal–ferromagnet thin films, which are composed of magnetic Co/Pt multilayers and an Au top-cladding layer. To the best of our knowledge, this is the first observation of AO-HDS in such a material system. The configuration of indirect optical excitation through a metallic layer has been employed to study the ultrafast demagnetization in ferrimagnetic and ferromagnetic materials, where a Cu,[38,39] Al,[40] or Au[41] layer coated on the top provides hot electrons to trigger the demagnetization. However, AO-HDS has not been observed in such metal–ferromagnet thin films. We have compared the switching effects of Co/Pt multilayers with and without the Au top-cladding layer under different conditions, including the laser repetition rate, scanning speed, and fluence. We find that the hybrid Co/Pt–Au samples show more obvious AO-HDS phenomena than those without the Au capping layer. We utilize an optomagnetic coupling model to reveal the critical role of the Au film in AO-HDS. The model indicates that the Au capping layer not only functions as a good heat sink but also prolongs the IFE-induced magnetic field to the picosecond timescale, which effectively triggers deterministic helicity-dependent switching.[20] Au has been widely used to implement a variety of plasmonic nanostructures to realize sub-diffraction-limited optical focusing effects. We envision that our current work would stimulate other work in the emerging area of magnetoplasmonics,[42–45] and further advance the technology of magnetic data storage with lower power and higher areal density by combining plasmonic structures with advanced magnetic materials.[46–48]

In our experiment, the laser system was based on a Ti:sapphire oscillator (Mira 900, Coherent, Inc) and a regenerative amplifier (RegA 9000, Coherent, Inc) pumped with a continuous wave laser (Verdi 18, Coherent, Inc). This system can generate 4 μJ pulses with a pulse width τ_{pulse} = 200 fs at the wavelength λ = 800 nm. The linearly polarized laser pulses were transformed to circularly polarized after passing through a quarter waveplate, and then focused by a lens with a focal length of 100 mm. The radius of the focused laser spot size was estimated to be r = 25.4 μm. A variable neutral density filter was used to control the intensity of incident pulses, and an electric shutter was used as an on/off switch to control laser pulses illuminating on the samples. We utilized a home-built MOKE microscope to observe the magnetization of domains in the out-of-plane direction. More details of the experimental setup can be found in Section S1 of the Supporting Information. All samples were grown by DC magnetron sputtering onto glass substrates at room temperature. The deposition was performed with an Ar pressure of 3×10^{-3} Torr and a background pressure of 10^{-7} Torr.

Figure 1a is the schematic illustration of the AO-HDS experiment. The hybrid metal–ferromagnet thin-film sample is exposed to RCP (denoted by σ^+)and LCP (denoted by σ^-) laser pulses, which induce reversible and robust magnetic switching. The hybrid sample has a stacked structure as Ta(3) Pt(0.7)[Co(0.8)/Pt(0.8)]$_3$Ta(3)Au(50) deposited on a clean glass substrate, where the numbers in brackets denote the layer thicknesses in nanometer. The 3 nm thick Ta films serve as the seeding and capping layers for the magnetic Co/Pt multilayer and a 50 nm Au layer is deposited at the top within the same sputtering process. Blue and red spins represent the magnetization pointing upwards (M^+) and downwards (M^-), respectively. The magnetic property of the hybrid metal–ferromagnet sample has been characterized by vibrating sample magnetometer (VSM) measurements for both in-plane and out-of-plane directions (Figure 1b). The dependence of the magnetization (normalized to the saturated magnetization M_s) with external magnetic field H shows that the hybrid sample has the easy axis along the out-of-plane direction and the hard axis along the in-plane direction, confirming its strong perpendicular magnetic anisotropy. The magnetic switching results can be imaged by an MOKE microscope. Depending on the magnetization orientation, linearly polarized light exhibits opposite polarization rotation angles that can be analyzed by a polarizer. Therefore, we can optically distinguish M^+ and M^- magnetizations, which show white and black contrast, respectively. When the σ^+ or σ^- laser pulses illuminate the hybrid metal–ferromagnet surface, the laser pulses penetrate through the Au top-cladding layer and induce laser heating and the inverse Faraday effect inside the Co/Pt multilayers, giving rise to pronounced and reversible AO-HDS phenomena. This allows us to write and erase arbitrary patterns, as presented in Figure 1c–e. The label "'NU," which stands for "Northeastern University," was written by σ^- and σ^+ laser pulses at the scanning speed of 100 μm s^{-1} on the sample. The laser fluence was about 3.02 mJ cm^{-2} and the laser repetition rate was 200 kHz. The letter "N" was written with σ^- laser pulses on magnetization initially pointing upward, and letter "U" was written with σ^+ laser beam on magnetization initially pointing downward. As shown in Figure 1d,e, "N" and "U" can be completely erased by flipping the helicity of the incident laser in comparison with that used in the writing process. These results unambiguously demonstrate well-controlled AO-HDS performance in the hybrid metal–ferromagnet sample.

Previous work on ferromagnetic materials, such Co/Pt multilayers[20,21] and granular FePt films,[23,24] demonstrated an accumulative feature in the AO-HDS process, where a certain number of laser pulses are required to establish the switching. To study switching features of the hybrid metal–ferromagnet thin films, we have conducted comprehensive studies on the influence of laser pulses per μm along the scanning direction on all-optical switching for the Co/Pt sample with 50 nm thick Au cladding layer. By controlling the repetition rate (10–200 kHz) and laser scanning speed (100–1000 μm s^{-1}), we characterized the switching performances when the number of pulses incident on the sample per μm ranged from 50 to 2000, while the laser fluence was fixed at 5.48 mJ cm^{-2}. The results for the hybrid Co/Pt–Au sample are shown in **Figure 2**a. For better visualizations, we have subtracted each MOKE figure with the corresponding background before laser scanning. The four columns present the switching results for four

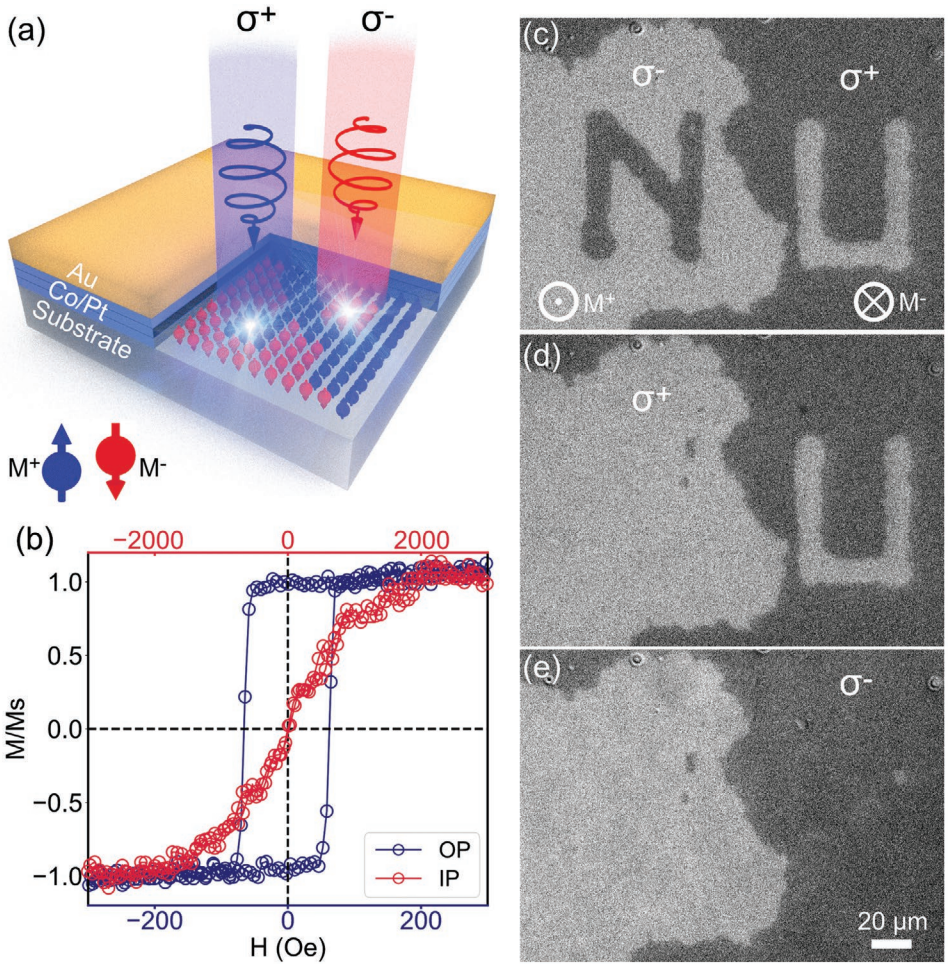

Figure 1. a) Schematic illustration of AO-HDS in a hybrid metal–ferromagnet material. The blue and red spins represent magnetization pointing upwards (M^+) and downwards (M^-), respectively. Deterministic magnetic switching can be induced by RCP (σ^+) and LCP (σ^-) laser pulses. b) VSM measurement result showing high perpendicular magnetic anisotropy of the hybrid metal–ferromagnet sample. c–e) MOKE images of the reversible AO-HDS in the hybrid Co/Pt–Au sample, exemplified by writing and erasing a label "NU" using a circular polarized laser. The label is written with laser fluence 3.02 mJ cm^{-2} at 200 kHz repetition rate. c) The letter "N" ("U") is written by σ^- (σ^+) laser pulses on initial M^+(M^-) magnetization. d) The letter "N" is erased by σ^+ laser pulses. e) The letter "U" is erased by σ^- laser pulses.

combinations of laser helicity and the initial magnetization, that is, (σ^+, M^-), (σ^-, M^-), (σ^+, M^+), and (σ^-, M^+). When the number of pulses per μm increases, the switched patterns for (σ^+, M^-) and (σ^-, M^+) transform from randomly distributed magnetic domains into helicity-dependent continuous lines. In contrast, for (σ^-, M^-) and (σ^+, M^+) configurations, the random magnetic domains gradually disappear. As a result, we obtain a distinct helicity-dependent difference in magnetization in the laser scanning regions when the number of pulses per μm is relatively large. It is noted that the switching at the ending point on the right of each scanning line is not dependent on helicity, which is instead caused by thermal demanganization.[1,12]

To quantitatively describe the switched results, we introduce a numerical method based on Gaussian fitting to calculate the switching ratio in each laser scanning experiment. The sign and amplitude of the switching ratio can fully characterize the magnetic switching performance. More specifically, a positive (negative) sign indicates switching on M^- (M^+) magnetization, and a larger amplitude implies more magnetization being switched. The detailed information about the calculation of the switching ratio can be found in Section S2 of the Supporting Information. In the experiments, we randomly selected three locations on the sample to repeat the experiments for each configuration with a certain number of laser pulses per μm, in order to avoid any potential influence of sample inhomogeneity. In Figure 2b, we plot the switching ratios of the four configurations versus the number of laser pulses per μm for the hybrid Co/Pt–Au sample. The switching ratio amplitudes for (σ^-, M^-) and (σ^+, M^+) gradually approach zero when the number of pulses per μm increases, while for (σ^-, M^+) and (σ^+, M^-) the amplitudes stay high, indicating helicity dependence in the magnetization switching becomes more pronounced. As a comparison, we have performed similar experiments on the Co/Pt control sample (that is, without the Au cladding layer only) under the laser fluence of 0.49 mJ cm^{-2} (see Section S3 of the Supporting Information). The corresponding switching ratios for the four configurations are plotted in Figure 2c. Comparing (σ^-, M^-) with (σ^+, M^-) or (σ^-, M^+) with (σ^+, M^+), we can only observe

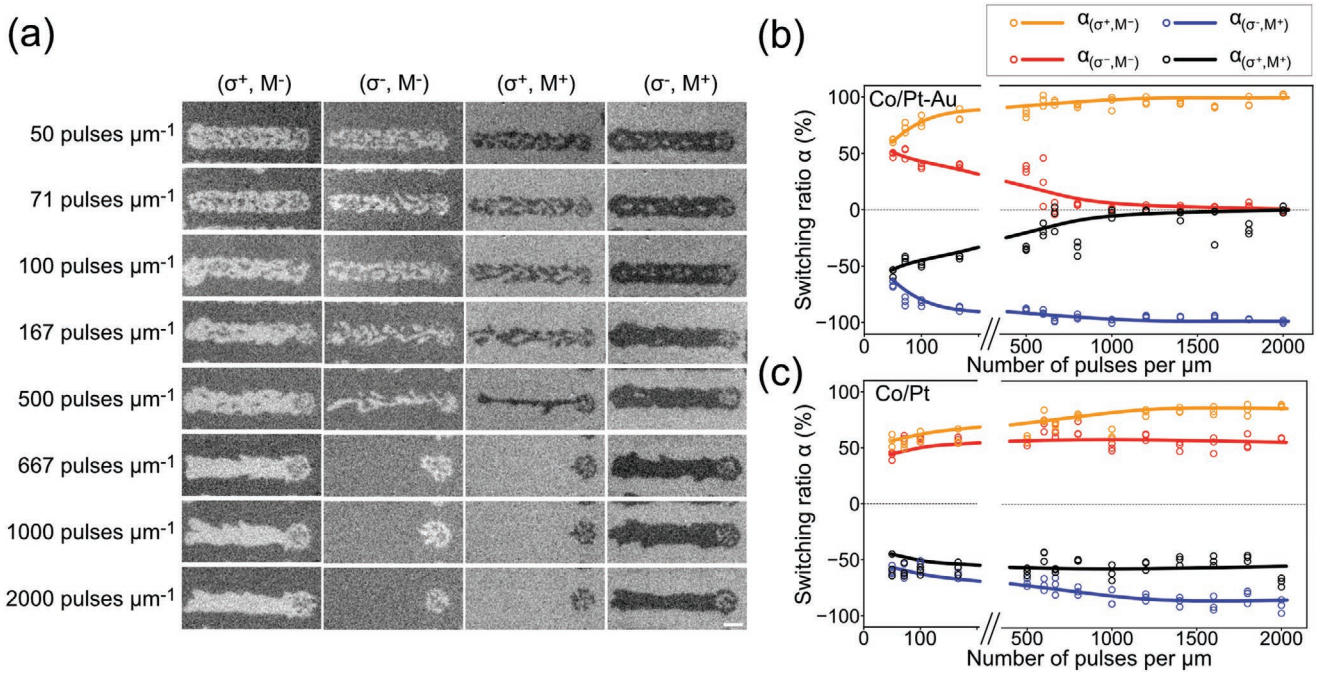

Figure 2. a) MOKE images of all-optical switching results when the number of laser pulses per μm increases. The sample configuration is Ta(3)Pt(0.7)[Co(0.8)/Pt(0.8)]$_3$Ta(3)Au(50), same as that in Figure 1, and the scans are performed with laser fluence of 5.48 mJ cm^{-2}. The scale bar in the bottom right corner is 20 μm. The switching ratio curves for the hybrid b) Co/Pt–Au and c) Co/Pt samples when the number of laser pulses per μm is changed from 50 to 2000. The curves for Co/Pt–Au sample indicate that the switching becomes more helicity dependent when the number of laser pulses per μm increases. While for the Co/Pt sample, the curves only show small dependence on the laser helicity. The solid lines are the guides to the eye.

weak helicity-dependent features. In addition, the switching ratio amplitudes for four configurations do not show strong dependence on the number of laser pulses per μm.

We have also compared the switching behaviors for the hybrid Co/Pt–Au and Co/Pt samples by varying laser fluences, as shown in **Figure 3**a,b. The four rows in each figure present the MOKE images of the magnetic patterns after laser scanning when the fluence is increased from the threshold that triggers switching to the value that thermally damages the samples. In the experiments, we kept the laser repetition rate at 200 kHz and scanning speed at 100 μm s^{-1}. We have conducted the experiments at three random locations on the samples with a certain initial magnetization as well as the fluence and helicity of the laser.

For the hybrid Co/Pt–Au sample (Figure 3a), a fluence of about 3.01 mJ cm^{-2} is the threshold to produce all-optical switching; while a laser beam with the fluence of 13.3 mJ cm^{-2} starts to thermally damage the sample, which is indicated by the gray shadows in the last row. The minimum laser fluence that triggers magnetic switching for the Co/Pt sample is about 0.296 mJ cm^{-2}. We have theoretically simulated the transmission of the Au layer at 800 nm wavelength. For a simple estimation, we considered a bare 50 nm thick Au film with the optical constant taken from Johnson and Christy's measurements,[49] through which the calculated transmission is 2.1%. For a more realistic estimation of the transmission, we have experimentally extracted the optical constant of our deposited 50 nm Au film, which is 0.44+3.5i. Subsequently, we have simulated the hybrid Co/Pt–Au thin-film structure, and the transmission is 1.2% after the 50 nm Au film. Considering either of the two transmission values, the switching threshold for the hybrid Co/Pt–Au sample should be more than ≈14.0 mJ cm^{-2}. However, experimentally we only need 3.01 mJ cm^{-2} to trigger magnetization switching in the hybrid sample. The result implies that the Au top-cladding layer reduces the expected switching threshold to achieve magnetic switching, and with such a moderate laser fluence, the switching becomes helicity dependent and pronounced.

Furthermore, we observe significant differences in the resulting magnetic patterns between the two samples. Over a large range of laser fluences, the hybrid Co/Pt–Au sample shows AO-HDS phenomena before the thermal damage. In other words, magnetic switching was achieved for (σ^+, M^-) and (σ^-, M^+), but not for (σ^+, M^+) and (σ^-, M^-). In contrast, the Co/Pt sample (Figure 3b) exhibits similar switched patterns for the four configurations at a given laser fluence. Interestingly, the pattern exhibited disordered stripe subdomains[50] when the fluence is 0.789 mJ cm^{-2} or above.

The switching ratios of the four configurations versus fluences are plotted in Figure 3c,d. For the hybrid Co/Pt–Au sample, the switching ratios for (σ^-, M^-) and (σ^+, M^+) are rather large, although they slightly decrease as the laser fluence increases. It is observed that as the laser fluence increases and enters the thermal damage zone (over 9.4 mJ cm^{-2}), the magnetic switching becomes not very stable. For (σ^-, M^-) and (σ^+, M^+) there are some portions of switched magnetization. As a result, the switching ratios are not very close to zero. Nevertheless, we achieve helicity-dependent switching even when the film was thermally damaged, as shown in the last row of Figure 3a, which demonstrates the robustness of AO-HDS in

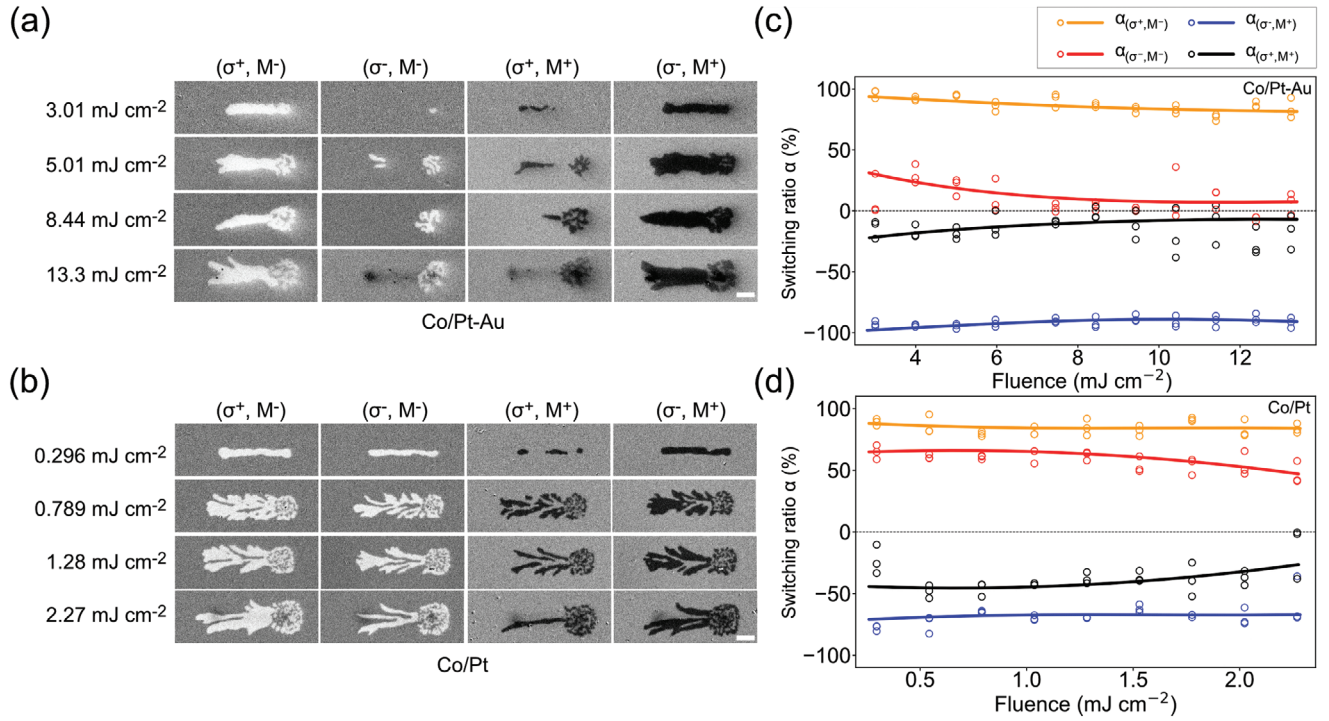

Figure 3. Laser scanning results for the hybrid a) Co/Pt–Au and b) Co/Pt samples when laser fluence is changed from the switching threshold to the thermal damage threshold. The scale bar in the bottom right corner is 20 µm. The switching ratios versus laser fluence for c) Co/Pt–Au and d) Co/Pt samples. The switching ratios for (σ^-, M^-) and (σ^+, M^+) configurations are close to zero for the hybrid Co/Pt–Au sample. However, significant portions of the magnetic domains are switched for these two configurations in the Co/Pt sample. The solid lines are the guides to the eye.

the Co/Pt–Au sample. In contrast, the switching characteristics for the Co/Pt sample are quite different. We do not observe clear helicity-dependent switched results, as can be seen by comparing (σ^-, M^-) with (σ^+, M^-) and (σ^-, M^+) with (σ^+, M^+).

To further examine the role of the Au top-cladding layer in this process, we have also studied Co/Pt samples capped with 10 and 30 nm Au layers, respectively. **Figure 4**a shows the scanning results of Co/Pt multilayers coated with 10 nm thick Au. With initial M^- magnetization, we hardly observe switching for both helicities at 0.249 mJ cm^{-2}, while helicity-dependent switching only exists when the fluence is within a small window near 0.257 mJ cm^{-2}. When the fluence increases

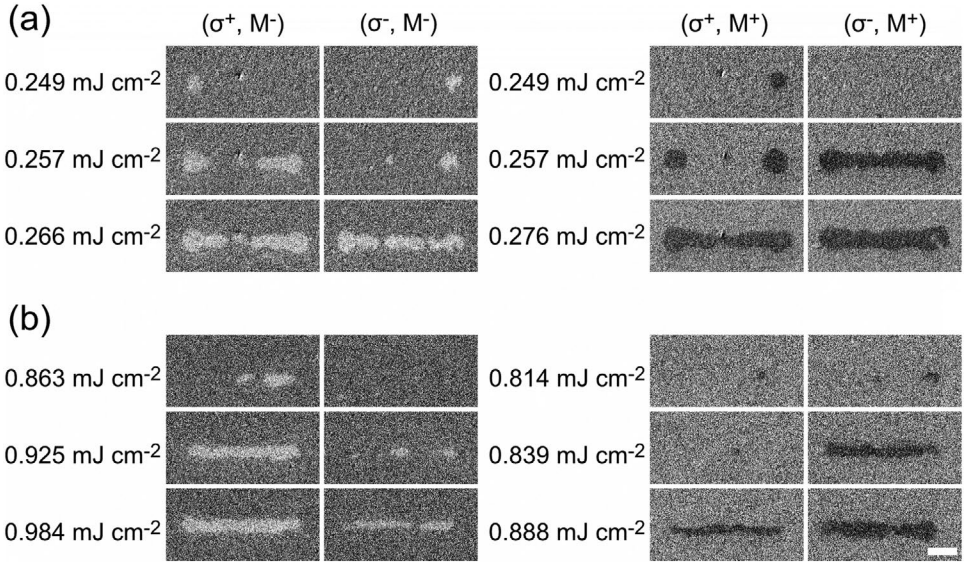

Figure 4. Laser scanning results for Co/Pt sample coated with a) 10 nm and b) 30 nm thick Au layers. The laser fluence was tuned so that the switched results show nonswitching, helicity-dependent switching and helicity-independent switching. The scale bar is 20 µm.

to 0.266 mJ cm^{-2}, both helicities will induce switching. Similar results are demonstrated with initial M^+magnetization, where we observe nonswitching, helicity-dependent switching, and helicity-independent switching at 0.249, 0.257, and 0.276 mJ cm^{-2}, respectively. Figure 4b presents the results of Co/Pt multilayers coated with 30 nm thick Au. We can observe helicity-dependent switching only within a small range near 0.925 mJ cm^{-2} on $M^-$and 0.839 mJ cm^{-2} on M^+. These results show clear difference compared with the results for Co/Pt coated with 50 nm Au, which exhibits AO-HDS within a considerably large fluence window as demonstrated in Figure 3a.

The AO-HDS process is closely related to the competition between the optothermal and optomagnetic effects of the laser pulses. Here we use an optomagnetic coupling[30] method that potentially explains the observed all-optical switching results in hybrid metal–ferromagnet materials, and the important role of the Au cladding layer. It is revealed that the Au top-cladding film facilitates the AO-HDS process in the following two ways: first, it works as a heat sink and cools down the magnetic film during the switching process. Second, it prolongs the induced magnetic flux that efficiently guides the deterministic switching. In our model, the prolonged magnetic flux density (B_i) is caused by Eddy current excited by the sub-picosecond IFE pulse. During the first a few hundreds of femtoseconds, the laser pulse irradiates the magnetic film and induces optomagnetic coupling through the inverse Faraday effect and wakes a loop current (Eddy current), both contributing to the overall induced B_i field. At the rising edge of the laser pulse, the induced B_i field ramps up together with the increasing electron temperature T_e and H_{IFE}. Meanwhile, the change of the magnetic flux (Φ_B) induces a vortex electric field E which displaces the electrons to form a loop current j that also contributes to the overall induced B_i field. According to Lenz's law, the direction of the B_i field created by the loop current j counteracts with the changing magnetic field, which causes a time delay between the peaks of the laser pulse and the overall induced B_i field. After H_{IFE} vanishes together with the laser pulse, the induced B_i field still exists because the loop current j sustained by the decreasing magnetic flux Φ_B. Because of the good electrical conductivity, the Eddy current inside the gold layer decays at the picosecond timescale. Details of the model are discussed in the Supporting Information. We have employed the macroscopic Landau Lifshitz Bloch equation[51–56] coupled with two temperature heat transfer equations.[2,11,29,57–59] The simulated structure is Co/Pt multilayers covered by a 50 nm thick Au film on the top. The laser has 200 kHz repetition rate and 200 fs pulse duration with 300 μm s^{-1} scanning speed. The effective magnetic field due to the inverse Faraday effect is chosen to be 100 G (mJ cm^{-2})$^{-1}$. To reduce the simulation time, we have limited the simulation domain to be 15 μm × 15 μm.

The electron and lattice temperatures at the center of Au and the Co/Pt films are plotted in **Figure 5**a. The femtosecond laser heats up the electrons, and electron temperature in the Au film ($T_{e,\,Au}$) rises rapidly above 1700 K because the Au film absorbs most of the laser power. The energetic electrons in the Au film raise the electron temperature in Co/Pt film ($T_{e,\,Co/Pt}$) via electron–electron interactions within the first 0.3 ps. The lattices gain energy via the electron–phonon coupling, and the lattice temperatures in the Au ($T_{l,\,Au}$) and Co/Pt ($T_{l,\,Co/Pt}$) films increase slowly because of the relatively large lattice heat capacities. The lattice temperature in Au ($T_{l,\,Au}$) does not change much due to the relatively small coupling coefficient at 4 × 10^{16} W (m^{3}K)$^{-1}$,[60] compared with the Co/Pt multilayers, which is 2.6 × 10^{18} W (m^{3}K)$^{-1}$.[29] The induced magnetic flux density (B_i) at the beam center arises from the inverse Faraday effect. Since Au has a larger electric conductivity compared to the Co/Pt film, B_i decays very slowly and lasts much longer than the 200 fs laser pulse. This prolonged B_i field guides the magnetization flipping when the electron temperature in the Co/Pt film falls below the Curie temperature (≈550 K). Figure 5b depicts the simulated laser scanning results when the initial magnetization points downward. The six frames show the evolution of magnetization after 1, 250, 500, 1000, 1500, and 2000 pulses, which on the time scale correspond to 5, 1250, 2500, 5000, 7500, and 10 000 μs. The center is thermally demagnetized, and a noise ranging from −10 to 10 G is introduced in the simulation. A video of the simulated laser scanning process is shown in Movie S1 (Supporting Information). Previous reports on Co/Pt samples demonstrated that efficient helicity-dependent magnetic switching can be observed only when the laser pulse duration is 2.0 ps or above.[20] While for shorter laser pulse durations in the range ≈100–500 fs, no consistent magnetic switching has been demonstrated in Co/Pt. This indicated that a sufficiently long duration of the induced magnetic flux is necessary for AO-HDS, which is consistent with our experimental observations.

To show the prolonged effective magnetic field induced by the cladding Au layer, in **Figure 6** we plot the magnetic flux density for the pure Co/Pt and hybrid Co/Pt–Au samples simulated by our model. The red spike presents the incident laser pulse. For the Co/Pt sample, the predicted decay of the induced magnetic field is about 1 ps, at a similar level considered by Vahaplar et al.[11] In sharp contrast, the results of the hybrid Co/Pt–Au sample show that a prolonged magnetic field amplitude remains ≈20% even after 25 ps. We infer that such a long-lived magnetic field drives the deterministic helicity-dependent switching in the Co/Pt–Au sample.

In summary, we have introduced a new material system, the hybrid metal–ferromagnet thin film, which shows a pronounced and stable AO-HDS effect. Compared to bare ferromagnet multiplayers, the scanned lines on hybrid metal–ferromagnet samples become more helicity dependent when the number of laser pulses per μm increases. Moreover, the AO-HDS in the hybrid sample is very stable over a wide range of laser fluences. Our numerical simulations, based on an optomagnetic coupling method, indicate that the Au top-cladding layer works as an efficient heat sink and also prolongs the IFE-induced magnetic field to the picosecond level, which substantially benefits the AO-HDS process. With the addition of the Au top-cladding layer, the hybrid metal–ferromagnet material demonstrates clear advantages and pronounced AO-HDS phenomena, which will potentially broaden the application of AO-HDS. The top-cladding material, Au, is one commonly used material to fabricate plasmonic nanostructures. Previous studies in magnetoplasmonics have demonstrated that Au plasmonic nanostructures, such as randomly distributed nanoparticles,[61–63] nanodisks,[64] and patterned gratings,[65–67] can be used to increase the Faraday/Kerr rotation induced by

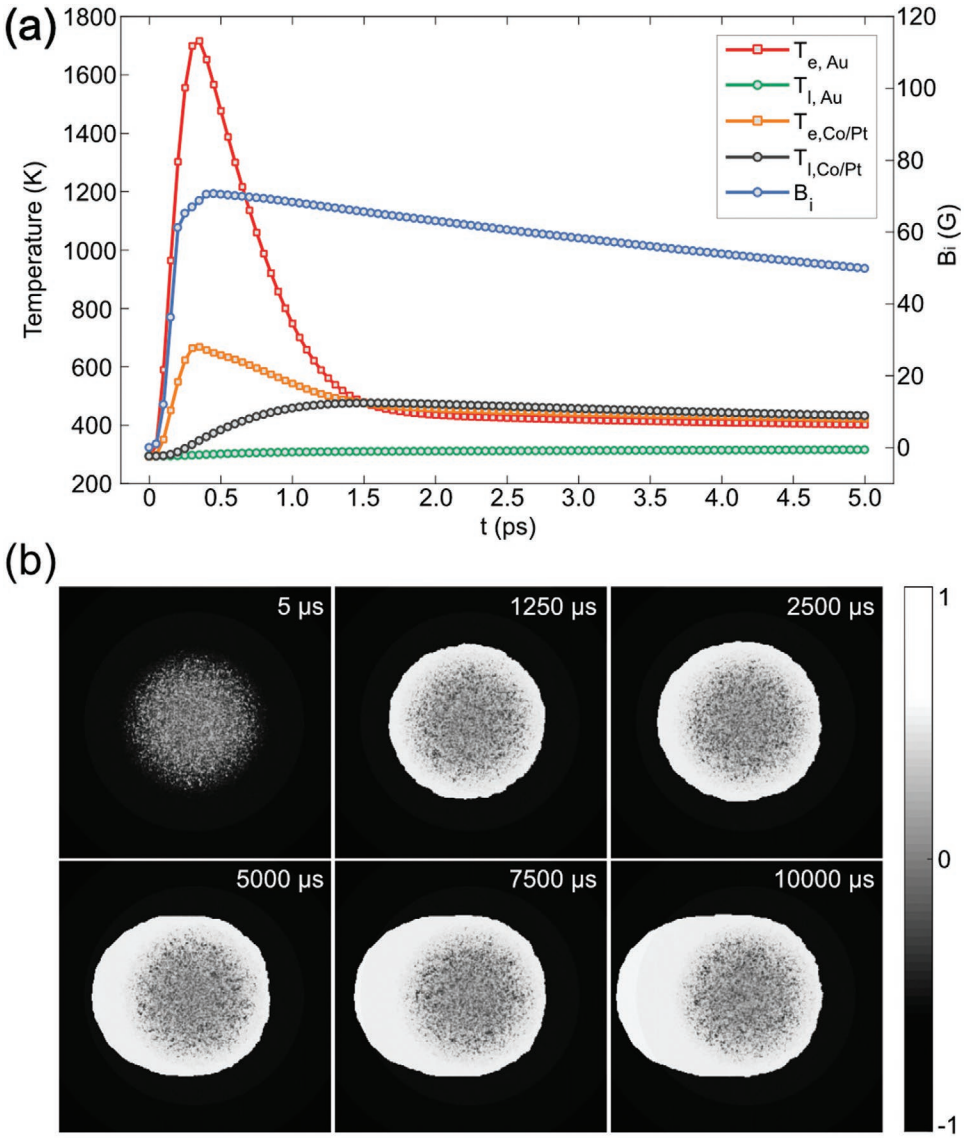

Figure 5. a) The electron and lattice temperatures (T_e and T_l) at the center of Au and Co/Pt films, and the induced magnetic flux density B_i at the center of the laser beam. b) Simulated AO-HDS results at 5, 1250, 2500, 5000, 7500, and 10 000 μs.

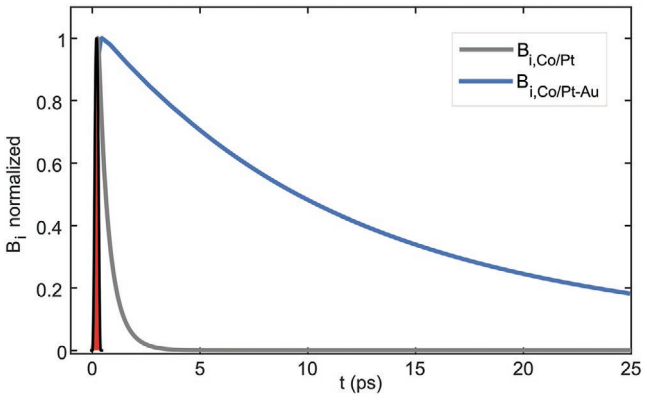

Figure 6. The simulated time-evolving magnetic flux density B_i for pure Co/Pt and hybrid Co/Pt–Au samples, compared with the incident laser pulse with duration of 200 fs.

magnetization. For these studies, the illuminated light is not sufficient to trigger magnetic switching. In the meantime, tremendous progress has been achieved in the area of heat-assisted magnetic switching (HAMR),[68–71] in which plasmonic nanostructures are applied to locally heat up the data bits, and the information is written by applying a small external magnetic field. This technique allows us to locally write data bits on the nanometer scale, which shows great potential to future storage technologies.

So far, plasmonics-enhanced all-optical switching was demonstrated for TbFeCo materials[48] but not for Co/Pt thin films, which are more often used in current storage devices. By patterning Au into different nanostructures, we expect to achieve strong local field enhancement within sub-diffraction-limited dimensions that results from the pronounced plasmonic resonances. This approach could be a critical leap forward enabling future plasmonics-integrated high-speed, low-power,

and high-density memory and storage technologies based on AO-HDS.

Supporting Information

Supporting Information is available from the Wiley Online Library or from the author.

Acknowledgements

The authors thank Prof. Hui Jia and Prof. Satoru Emori for the assistance at the early stage of this work. The authors also appreciate the helpful discussion with Prof. Eric Fullerton. Y.L. acknowledges the financial support of NSF DMR-1654192. L.P. acknowledges the financial support of NSF CMMI-1554189. A.B. and P.C. were supported by NSF CHE-1764221.

Conflict of Interest

The authors declare no conflict of interest.

Keywords

all-optical switching, data storage, helicity, laser pulses, magnetic materials, ultrafast

Received: March 5, 2020
Published online:

[1] C. D. Stanciu, F. Hansteen, A. V. Kimel, A. Kirilyuk, A. Tsukamoto, A. Itoh, Th. Rasing, *Phys. Rev. Lett.* **2007**, *99*, 047601.
[2] K. Vahaplar, A. M. Kalashnikova, A. V. Kimel, D. Hinzke, U. Nowak, R. Chantrell, A. Tsukamoto, A. Itoh, A. Kirilyuk, Th. Rasing, *Phys. Rev. Lett.* **2009**, *103*, 117201.
[3] S. Alebrand, M. Gottwald, M. Hehn, D. Steil, M. Cinchetti, D. Lacour, E. E. Fullerton, M. Aeschlimann, S. Mangin, *Appl. Phys. Lett.* **2012**, *101*, 162408.
[4] A. Hassdenteufel, B. Hebler, C. Schubert, A. Liebig, M. Teich, M. Helm, M. Aeschlimann, M. Albrecht, R. Bratschitsch, *Adv. Mater.* **2013**, *25*, 3122.
[5] A. Hassdenteufel, C. Schubert, J. Schmidt, P. Richter, D. R. T. Zahn, G. Salvan, M. Helm, R. Bratschitsch, M. Albrecht, *Appl. Phys. Lett.* **2014**, *105*, 112403.
[6] J. Hohlfeld, C. D. Stanciu, A. Rebei, *Appl. Phys. Lett.* **2009**, *94*, 152504.
[7] D. Steil, S. Alebrand, A. Hassdenteufel, M. Cinchetti, M. Aeschlimann, *Phys. Rev. B* **2011**, *84*, 224408.
[8] A. Hassdenteufel, J. Schmidt, C. Schubert, B. Hebler, M. Helm, M. Albrecht, R. Bratschitsch, *Phys. Rev. B* **2015**, *91*, 104431.
[9] A. V. Kimel, A. Kirilyuk, P. A. Usachev, R. V. Pisarev, A. M. Balbashov, Th. Rasing, *Nature* **2005**, *435*, 655.
[10] S. Alebrand, A. Hassdenteufel, D. Steil, M. Cinchetti, M. Aeschlimann, *Phys. Rev. B* **2012**, *85*, 092401.
[11] K. Vahaplar, A. M. Kalashnikova, A. V. Kimel, S. Gerlach, D. Hinzke, U. Nowak, R. Chantrell, A. Tsukamoto, A. Itoh, A. Kirilyuk, Th. Rasing, *Phys. Rev. B* **2012**, *85*, 104402.
[12] A. R. Khorsand, M. Savoini, A. Kirilyuk, A. V. Kimel, A. Tsukamoto, A. Itoh, Th. Rasing, *Phys. Rev. Lett.* **2012**, *108*, 127205.
[13] M. Savoini, R. Medapalli, B. Koene, A. R. Khorsand, L. Le Guyader, L. Duò, M. Finazzi, A. Tsukamoto, A. Itoh, F. Nolting, A. Kirilyuk, A. V. Kimel, Th. Rasing, *Phys. Rev. B* **2012**, *86*, 140404(R).
[14] C. Schubert, A. Hassdenteufel, P. Matthes, J. Schmidt, M. Helm, R. Bratschitsch, M. Albrecht, *Appl. Phys. Lett.* **2014**, *104*, 082406.
[15] L. Le Guyader, M. Savoini, S. El Moussaoui, M. Buzzi, A. Tsukamoto, A. Itoh, A. Kirilyuk, T. Rasing, A. V. Kimel, F. Nolting, *Nat. Commun.* **2015**, *6*, 5839.
[16] A. Hassdenteufel, C. Schubert, B. Hebler, H. Schultheiss, J. Fassbender, M. Albrecht, R. Bratschitsch, *Opt. Express* **2014**, *22*, 10017.
[17] C.-H. Lambert, S. Mangin, B. S. D. C. S. Varaprasad, Y. K. Takahashi, M. Hehn, M. Cinchetti, G. Malinowski, K. Hono, Y. Fainman, M. Aeschlimann, E. E. Fullerton, *Science* **2014**, *345*, 1337.
[18] Yu. Tsema, G. Kichin, O. Hellwig, V. Mehta, A. V. Kimel, A. Kirilyuk, Th. Rasing, *Appl. Phys. Lett.* **2016**, *109*, 072405.
[19] M. S. El Hadri, M. Hehn, P. Pirro, C.-H. Lambert, G. Malinowski, E. E. Fullerton, S. Mangin, *Phys. Rev. B* **2016**, *94*, 064419.
[20] R. Medapalli, D. Afanasiev, D. K. Kim, Y. Quessab, S. Manna, S. A. Montoya, A. Kirilyuk, Th. Rasing, A. V. Kimel, E. E. Fullerton, *Phys. Rev. B* **2017**, *96*, 224421.
[21] M. S. E. Hadri, P. Pirro, C.-H. Lambert, S. Petit-Watelot, Y. Quessab, M. Hehn, F. Montaigne, G. Malinowski, S. Mangin, *Phys. Rev. B: Condens. Matter Mater. Phys.* **2016**, *94*, 64412.
[22] Y. Quessab, R. Medapalli, M. S. El Hadri, M. Hehn, G. Malinowski, E. E. Fullerton, S. Mangin, *Phys. Rev. B* **2018**, *97*, 054419.
[23] Y. K. Takahashi, R. Medapalli, S. Kasai, J. Wang, K. Ishioka, S. H. Wee, O. Hellwig, K. Hono, E. E. Fullerton, *Phys. Rev. Appl.* **2016**, *6*, 054004.
[24] R. John, M. Berritta, D. Hinzke, C. Müller, T. Santos, H. Ulrichs, P. Nieves, J. Walowski, R. Mondal, O. Chubykalo-Fesenko, J. McCord, P. M. Oppeneer, U. Nowak, M. Münzenberg, *Sci. Rep.* **2017**, *7*, 4114.
[25] M. S. El Hadri, P. Pirro, C.-H. Lambert, N. Bergeard, S. Petit-Watelot, M. Hehn, G. Malinowski, F. Montaigne, Y. Quessab, R. Medapalli, E. E. Fullerton, S. Mangin, *Appl. Phys. Lett.* **2016**, *108*, 092405.
[26] M. Vomir, M. Albrecht, J.-Y. Bigot, *Appl. Phys. Lett.* **2017**, *111*, 242404.
[27] L. P. Pitaevskii, *J. Exptl. Theoret. Phys.* **1961**, *12*, 1008.
[28] J. P. van der Ziel, P. S. Pershan, L. D. Malmstrom, *Phys. Rev. Lett.* **1965**, *15*, 190.
[29] T. D. Cornelissen, R. Cordoba, B. Koopmans, *Appl. Phys. Lett.* **2016**, *108*, 142405.
[30] Z. Du, C. Chen, F. Cheng, Y. Liu, L. Pan, *Sci. Rep.* **2017**, *7*, 13513.
[31] M. O. A. Ellis, E. E. Fullerton, R. W. Chantrell, *Sci. Rep.* **2016**, *6*, srep30522.
[32] J. Gorchon, Y. Yang, J. Bokor, *Phys. Rev. B* **2016**, *94*, 020409(R).
[33] G. P. Zhang, Y. H. Bai, T. F. George, *EPL* **2016**, *115*, 57003.
[34] T. J. Huisman, R. V. Mikhaylovskiy, J. D. Costa, F. Freimuth, E. Paz, J. Ventura, P. P. Freitas, S. Blügel, Y. Mokrousov, Th. Rasing, A. V. Kimel, *Nat. Nanotechnol.* **2016**, *11*, 455.
[35] G.-M. Choi, A. Schleife, D. G. Cahill, *Nat. Commun.* **2017**, *8*, 15085.
[36] M. Battiato, K. Carva, P. M. Oppeneer, *Phys. Rev. Lett.* **2010**, *105*, 027203.
[37] E. Turgut, C. La-o-vorakiat, J. M. Shaw, P. Grychtol, H. T. Nembach, D. Rudolf, R. Adam, M. Aeschlimann, C. M. Schneider, T. J. Silva, M. M. Murnane, H. C. Kapteyn, S. Mathias, *Phys. Rev. Lett.* **2013**, *110*, 197201.
[38] G.-M. Choi, B.-C. Min, K.-J. Lee, D. G. Cahill, *Nat. Commun.* **2014**, *5*, 4334.
[39] N. Bergeard, M. Hehn, S. Mangin, G. Lengaigne, F. Montaigne, M. L. M. Lalieu, B. Koopmans, G. Malinowski, *Phys. Rev. Lett.* **2016**, *117*, 147203.
[40] B. Vodungbo, B. Tudu, J. Perron, R. Delaunay, L. Müller, M. H. Berntsen, G. Grübel, G. Malinowski, C. Weier, J. Gautier, G. Lambert, P. Zeitoun, C. Gutt, E. Jal, A. H. Reid, P. W. Granitzka, N. Jaouen, G. L. Dakovski, S. Moeller, M. P. Minitti, A. Mitra, S. Carron, B. Pfau, C. von, K. Schmising, M. Schneider, S. Eisebitt, J. Lüning, *Sci. Rep.* **2016**, *6*, 18970.

[41] R. B. Wilson, J. Gorchon, Y. Yang, C.-H. Lambert, S. Salahuddin, J. Bokor, *Phys. Rev. B* **2017**, *95*, 180409(R).
[42] V. V. Temnov, G. Armelles, U. Woggon, D. Guzatov, A. Cebollada, A. Garcia-Martin, J.-M. Garcia-Martin, T. Thomay, A. Leitenstorfer, R. Bratschitsch, *Nat. Photonics* **2010**, *4*, 107.
[43] G. Armelles, A. Cebollada, A. García-Martín, M. U. González, *Adv. Opt. Mater.* **2013**, *1*, 10.
[44] B. Caballero, A. García-Martín, J. C. Cuevas, *ACS Photonics* **2016**, *3*, 203.
[45] Z. Tang, L. Chen, C. Zhang, S. Zhang, C. Lei, D. Li, S. Wang, S. Tang, Y. Du, *Opt. Lett.* **2018**, *43*, 5090.
[46] K. Nakagawa, Y. Ashizawa, S. Ohnuki, A. Itoh, A. Tsukamoto, *J. Appl. Phys.* **2011**, *109*, 07B735.
[47] B. Koene, M. Savoini, A. V. Kimel, A. Kirilyuk, T. Rasing, *Appl. Phys. Lett.* **2012**, *101*, 013115.
[48] T.-M. Liu, T. Wang, A. H. Reid, M. Savoini, X. Wu, B. Koene, P. Granitzka, C. E. Graves, D. J. Higley, Z. Chen, G. Razinskas, M. Hantschmann, A. Scherz, J. Stöhr, A. Tsukamoto, B. Hecht, A. V. Kimel, A. Kirilyuk, T. Rasing, H. A. Dürr, *Nano Lett.* **2015**, *15*, 6862.
[49] P. B. Johnson, R. W. Christy, *Phys. Rev. B* **1972**, *6*, 4370.
[50] F. Hoveyda, E. Hohenstein, S. Smadici, *J. Phys.: Condens. Matter* **2017**, *29*, 225801.
[51] D. A. Garanin, *Phys. Rev. B* **1997**, *55*, 3050.
[52] J. L. García-Palacios, F. J. Lázaro, *Phys. Rev. B* **1998**, *58*, 14937.
[53] O. Chubykalo-Fesenko, U. Nowak, R. W. Chantrell, D. Garanin, *Phys. Rev. B* **2006**, *74*, 094436.
[54] U. Atxitia, O. Chubykalo-Fesenko, R. W. Chantrell, U. Nowak, A. Rebei, *Phys. Rev. Lett.* **2009**, *102*, 057203.
[55] C. Schieback, D. Hinzke, M. Kläui, U. Nowak, P. Nielaba, *Phys. Rev. B* **2009**, *80*, 214403.
[56] W. Zhu, D. Xiao, Y. Liu, S. J. Gong, C.-G. Duan, *Sci. Rep.* **2015**, *4*, 4117.
[57] E. Beaurepaire, J.-C. Merle, A. Daunois, J.-Y. Bigot, *Phys. Rev. Lett.* **1996**, *76*, 4250.
[58] N. Kazantseva, U. Nowak, R. W. Chantrell, J. Hohlfeld, A. Rebei, *EPL* **2008**, *81*, 27004.
[59] B. Koopmans, G. Malinowski, F. Dalla Longa, D. Steiauf, M. Fähnle, T. Roth, M. Cinchetti, M. Aeschlimann, *Nat. Mater.* **2010**, *9*, 259.
[60] Z. Lin, L. V. Zhigilei, V. Celli, *Phys. Rev. B* **2008**, *77*, 075133.
[61] R. Fujikawa, A. V. Baryshev, J. Kim, H. Uchida, M. Inoue, *J. Appl. Phys.* **2008**, *103*, 07D301.
[62] H. Uchida, Y. Masuda, R. Fujikawa, A. V. Baryshev, M. Inoue, *J. Magn. Magn. Mater.* **2009**, *321*, 843.
[63] S. Tkachuk, G. Lang, C. Krafft, O. Rabin, I. Mayergoyz, *J. Appl. Phys.* **2011**, *109*, 07B717.
[64] B. Sepúlveda, J. B. González-Díaz, A. García-Martín, L. M. Lechuga, G. Armelles, *Phys. Rev. Lett.* **2010**, *104*, 147401.
[65] L. E. Kreilkamp, V. I. Belotelov, J. Y. Chin, S. Neutzner, D. Dregely, T. Wehlus, I. A. Akimov, M. Bayer, B. Stritzker, H. Giessen, *Phys. Rev. X* **2013**, *3*, 041019.
[66] N. E. Khokhlov, A. R. Prokopov, A. N. Shaposhnikov, V. N. Berzhansky, M. A. Kozhaev, S. N. Andreev, A. P. Ravishankar, V. G. Achanta, D. A. Bykov, A. K. Zvezdin, V. I. Belotelov, *J. Phys. D: Appl. Phys.* **2015**, *48*, 095001.
[67] O. V. Borovkova, H. Hashim, M. A. Kozhaev, S. A. Dagesyan, A. Chakravarty, M. Levy, V. I. Belotelov, *Appl. Phys. Lett.* **2018**, *112*, 063101.
[68] W. A. Challener, C. Peng, A. V. Itagi, D. Karns, W. Peng, Y. Peng, X. Yang, X. Zhu, N. J. Gokemeijer, Y.-T. Hsia, G. Ju, R. E. Rottmayer, M. A. Seigler, E. C. Gage, *Nat. Photonics* **2009**, *3*, 220.
[69] B. C. Stipe, T. C. Strand, C. C. Poon, H. Balamane, T. D. Boone, J. A. Katine, J.-L. Li, V. Rawat, H. Nemoto, A. Hirotsune, O. Hellwig, R. Ruiz, E. Dobisz, D. S. Kercher, N. Robertson, T. R. Albrecht, B. D. Terris, *Nat. Photonics* **2010**, *4*, 484.
[70] T. Matsumoto, F. Akagi, M. Mochizuki, H. Miyamoto, B. Stipe, *Opt. Express* **2012**, *20*, 18946.
[71] A. Q. Wu, Y. Kubota, T. Klemmer, T. Rausch, C. Peng, Y. Peng, D. Karns, X. Zhu, Y. Ding, E. K. C. Chang, Y. Zhao, H. Zhou, K. Gao, J.-U. Thiele, M. Seigler, G. Ju, E. Gage, *IEEE Trans. Magn.* **2013**, *49*, 779.

